VIP Heterojunctions Very Important Paper

DOI: 10.1002/ange.201408882

Solution-Grown Organic Single-Crystalline Donor–Acceptor Heterojunctions for Photovoltaics**

Hanying Li, Congcheng Fan, Weifei Fu, Huolin L. Xin, and Hongzheng Chen**

Abstract: *Organic single crystals are ideal candidates for high-performance photovoltaics due to their high charge mobility and long exciton diffusion length; however, they have not been largely considered for photovoltaics due to the practical difficulty in making a heterojunction between donor and acceptor single crystals. Here, we demonstrate that extended single-crystalline heterojunctions with a consistent donor-top and acceptor-bottom structure throughout the substrate can be simply obtained from a mixed solution of C_{60} (acceptor) and 3,6-bis(5-(4-n-butylphenyl)thiophene-2-yl)-2,5-bis(2-ethylhexyl)pyrrolo[3,4-c]pyrrole-1,4-dione (donor). 46 photovoltaic devices were studied with the power conversion efficiency of (0.255 ± 0.095) % under 1 sun, which is significantly higher than the previously reported value for a vapor-grown organic single-crystalline donor–acceptor heterojunction (0.007 %). As such, this work opens a practical avenue for the study of organic photovoltaics based on single crystals.*

Photovoltaic effects typically originate from the asymmetric structures that enable the separation of electrons and holes. Within these optoelectronically functional structures, donor–acceptor heterojunctions have been widely used for organic photovoltaics to dissociate illumination-generated excitons into separated electrons and holes. Initially, planar heterojunctions (Figure 1 a) with laminated organic donor and acceptor layers were found to generate photocurrents with a power conversion efficiency (PCE) of about 1 %.[1] Evolving from the planar structures, bulk heterojunctions (BHJs, Figure 1 b) where donor and acceptor form three-dimensional (3D) interpenetrating networks to facilitate the exciton dissociation, subsequently, became dominant.[2] Essentially, the BHJ architecture bypasses the disadvantage of the disorder-limited short exciton diffusion length (about 3–50 nm)[3] of typical organic thin films, leading to greatly improved PCE values of about 10 %.[4]

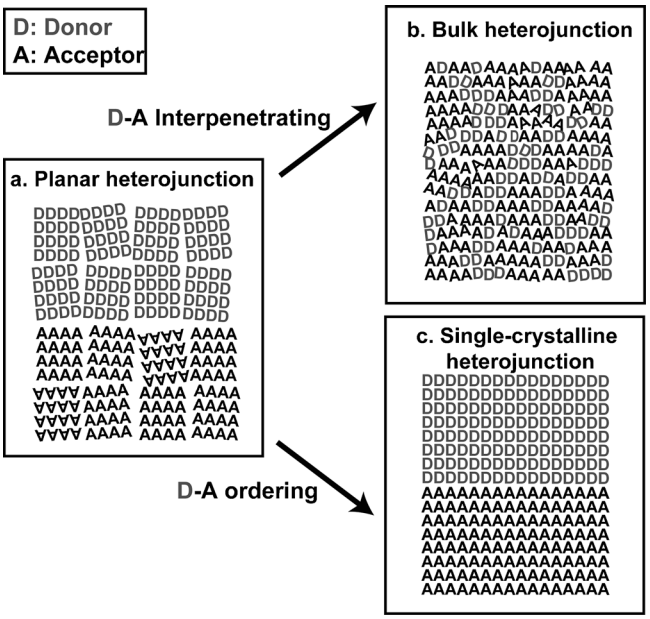

Figure 1. Evolution of the structure of organic donor–acceptor heterojunctions for photovoltaics. The donor (D) phase and the acceptor (A) phase in a planar heterojunction (a) interpenetrate into each other to form a bulk heterojunction (b), while the crystallographic ordering of these two phases results in a single-crystalline heterojunction (c).

Despite the great success of BHJs, this is not the only way to improve exciton dissociation. Instead of bypassing the shortcoming of short exciton diffusion length, efforts have been made to directly improve the exciton diffusion by increasing the ordering of molecular packing. It has been demonstrated in several materials[3b,c,5] that more extended crystallinity leads to longer exciton diffusion lengths that reach up to several microns in the case of rubrene single crystals.[6] As a result, highly crystalline and even single-crystalline organic materials were used to fabricate solar cells.[5b,7] In addition to the longer exciton diffusion, another advantage of highly crystalline materials is the fast charge transport[8] that is equally important for photocurrent generation. Ideally, single-crystalline heterojunctions (Figure 1 c), in which single crystals of donor and acceptor are in contact with each other, are expected to exhibit a superior photovoltaic effect due to their highly ordered molecular packing. However, single-crystalline donor–acceptor heterojunctions are difficult to fabricate. Only in two cases were

[*] Prof. H. Y. Li, C. C. Fan, W. F. Fu, Prof. H. Z. Chen
MOE Key Laboratory of Macromolecular Synthesis and Functionalization, State Key Laboratory of Silicon Materials
Department of Polymer Science and Engineering
Zhejiang University, Hangzhou 310027 (P.R. China)
E-mail: hanying_li@zju.edu.cn
hzchen@zju.edu.cn
Dr. H. L. Xin
Center for Functional Nanomaterials
Brookhaven National Laboratory, Upton, NY 11973 (USA)

[**] We thank D. J. Lipomi for discussions. This work was supported by the 973 Program (2014CB643503), the National Natural Science Foundation of China (51222302, 51373150, 51461165301, 91233114), the Zhejiang Province Natural Science Foundation (LZ13E030002), and Fundamental Research Funds for the Central Universities. H.L.X. is supported by the Center for Functional Nanomaterials, Brookhaven National Laboratory, which is supported by the U.S. Department of Energy, Office of Basic Energy Sciences, under Contract No. DE-AC02-98CH10886.

Supporting information for this article is available on the WWW under http://dx.doi.org/10.1002/anie.201408882.

single-crystalline heterojunctions successfully prepared from vapors, with relatively small active areas of about tens of μm^2.[7b,f] These small-sized junctions resulted in difficult device fabrication (e.g., electrode deposition near the junction) and a relatively low PCE of 0.007 % under 1 sun (1 sun is typically defined as the nominal full sunlight intensity on a bright clear day on Earth, which amounts to 100 mW cm^{-2}).[7b] Instead of vapor, crystallization from solution might be a better approach to prepare single-crystalline donor–acceptor heterojunctions and their devices. Previously, we developed a droplet-pinned crystallization (DPC) method to prepare well-aligned organic single crystals and their heterojunctions from solutions.[9] In this work, using this solution method, we obtain single-crystalline donor–acceptor heterojunctions of 3,6-bis(5-(4-*n*-butylphenyl)thiophene-2-yl)-2,5-bis(2-ethylhexyl)pyrrolo[3,4-*c*]pyrrole-1,4-dione (DPP-PR) and C_{60} and we achieve a greatly improved PCE as high as 0.46 %.

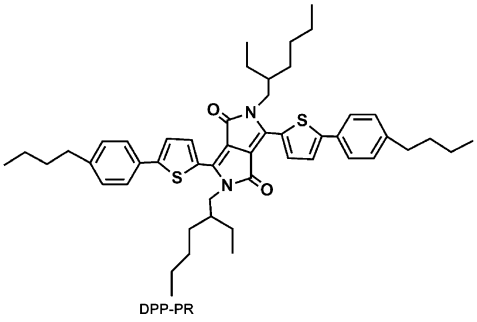

DPP-PR and C_{60} were used to grow single-crystalline donor–acceptor heterojunctions. Diketopyrrolopyrrole (DPP) derivatives are widely used donors in organic solar cells[4g,10] and DPP-PR is a reported donor material for BHJ solar cells.[11] C_{60} and its derivatives are the most frequently used acceptors for organic solar cells.[12] Accordingly, DPP-PR and C_{60} were used to grow single-crystalline donor–acceptor heterojunctions. Before growing heterojunctions, we first prepared single-component crystals of DPP-PR ribbons and C_{60} ribbons separately using the DPC method and obtained their well-aligned single crystals (Figure S1). Next, a mixed solution of DPP-PR and C_{60} was prepared. The receding of a pinned droplet of the mixed solution resulted in ribbonlike crystals (Figure 2 a,b) which grew in a bilayer fashion as indicated clearly by the atomic force microscopy (AFM) height profile (Figure 2 d). The ribbons were colored and a few microns to tens of microns wide, with the brown wider ribbons on top of the blue ones. The colors are consistent with the colors of DPP-PR (brown) and C_{60} (blue) (Figure S1 a,b). The thickness of the top and bottom layers is (35.5 ± 3.8) nm and (21.8 ± 2.0) nm, respectively. In order to characterize the chemical composition of the overlapping bilayers, the crystals were examined with a Raman intensity map in the 1488–1556 cm^{-1} and 1444–1483 cm^{-1} regions (characteristic Raman shifts of DPP-PR and C_{60} respectively, Figure S2). The green mapping marks the region of DPP-PR, while the yellow one that of C_{60} (Figure 2 a,b). Clearly, the top

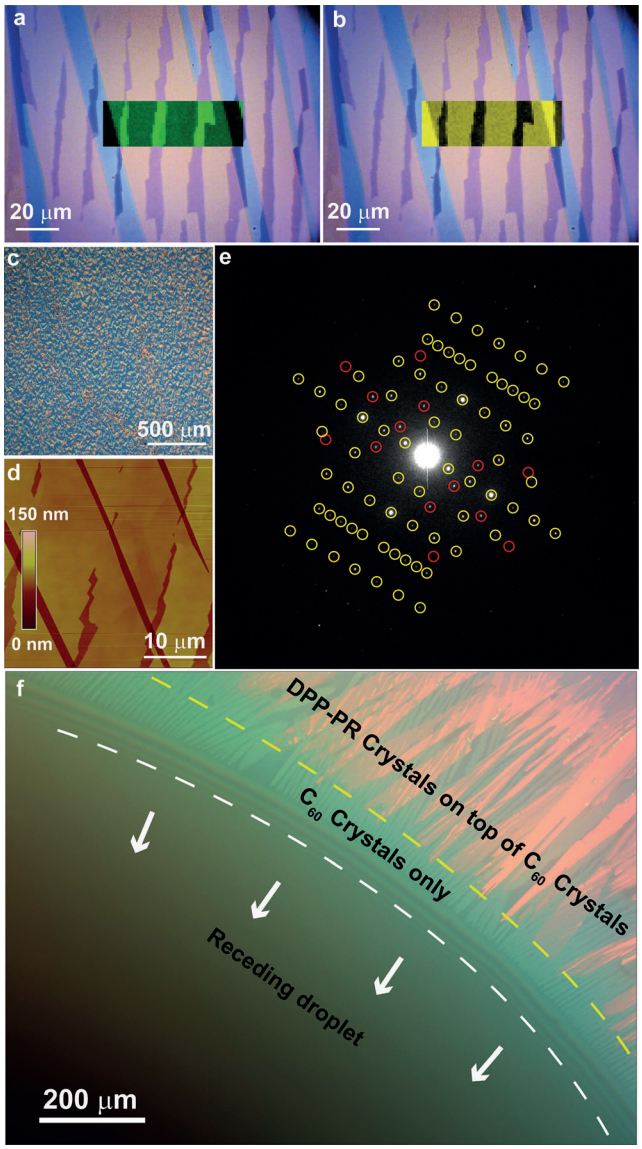

Figure 2. The morphology and crystalline structure of DPP-PR ribbon and C_{60} ribbon single-crystalline donor–acceptor heterojunctions. a,b) Optical microscopy (OM) images. Insets: Raman intensity maps in an area containing both brown and blue ribbons, with the green and yellow regions showing the Raman signals from DPP-PR and C_{60}, respectively. c) An OM image of mixed solids dried from a droplet of a mixed solution of DPP-PR and C_{60} without using the pinner to pin the droplet. d) An AFM image showing a bilayer structure. e) An SAED pattern showing two sets of diffraction spots highlighted by the yellow and red circles. f) An OM snapshot of a receding droplet of the mixed solution of DPP-PR and C_{60}. A movie recording the droplet receding is shown in Movie S1.

brown layers are assigned to DPP-PR crystals and the bottom blue layers are C_{60}. Also, Raman mapping at randomly selected different locations provided consistent results of the DPP-PR-top and C_{60}-bottom structure (Figure S3). The crystallography of the bilayers was further investigated. Selected-area electron diffraction (SAED) of the bilayers showed two sets of diffraction spots (Figure 2 e and Figure S4, yellow and red circles), indicative of two different single crystals. Therefore, OM, Raman, AFM, and SAED data

demonstrate that we obtained donor–acceptor single-crystalline heterojunctions with DPP-PR on top of C_{60}.

Considering that single crystals usually grow from relatively pure media into relatively pure solids, the formation of bilayer single crystals from a mixed solution demands the understanding of their formation mechanism. In a control experiment, a drop of the mixed solution was dried under the same conditions except that the pinner, the key component of the DPC method, was missing. As a result, we obtained a random mixture of DPP-PR and C_{60} (Figure 2c), suggesting severe mutual disturbance in the crystallization of DPP-PR and C_{60}. The discrepancy between the random mixture and the well-aligned bilayer single crystals raised two questions: 1) How does the DPC method avoid the mutual disturbance of the growing DPP-PR and C_{60} crystals? 2) Why are the C_{60} crystals always on the bottom while DPP-PR is on the top?

The formation mechanism of the heterojunctions was studied by videotaping the receding droplet of the mixed solution (Movie S1). We observed sequential crystallization events where one crystal grew first and the other crystal followed, similar to previous observations of the mixed solution of 2,7-dioctyl[1]benzothieno[3,2-*b*][1]benzothiophene (C8-BTBT) and C_{60}.[9b] In a snapshot (Figure 2f) of the receding droplet, three regions were clearly recognized near the contact line: the droplet, blue C_{60} crystals only, and brown DPP-PR crystals on top of the blue C_{60} crystals. Based on the relative positions of these regions, it is concluded that the blue C_{60} crystals grew first; then the brown DPP-PR crystals nucleated heterogeneously on the C_{60} crystals (Figure S5). These sequential crystallization events avoid the mutual disturbance of the growing crystals to give the overlapping bilayer single crystals but not a mixture of two solids. Furthermore, the sequential crystallization determines the donor-top and acceptor-bottom configuration because the first growing crystal, C_{60} acceptor in this case, will be always on the bottom. Interestingly, the relative positions of the DPP-PR and C_{60} can be switched by modifying the sequential crystallization. When the concentration ratio of DPP-PR to C_{60} was as high as 4:1, DPP-PR, instead of C_{60}, crystallized first and we obtained DPP-PR-bottom and C_{60}-top structure (Figure S6).

After obtaining the heterojunctions, we proceeded to examine their electronic properties. We first studied the transport properties using field-effect transistors (FETs). The typical transfer and output characteristics of the devices are shown in Figure S7a–d, in which ambipolar charge transport behavior was observed. 40 devices were tested to derive the statistics of the mobility values (Figure S7e,f). For hole transport, an average hole mobility (μ_h) of (0.0026 ± 0.0015) $cm^2 V^{-1} s^{-1}$ (range: 0.0007–0.0061), on-to-off current ratio (I_{on}/I_{off}) > 10, and threshold voltage (V_T) between −65.3 and −87.7 V were obtained. For electron transport, we achieved an average electron mobility (μ_e) of (0.28 ± 0.12) $cm^2 V^{-1} s^{-1}$ (range: 0.13–0.59), $I_{on}/I_{off} > 10^3$,and V_T between 32.5 and 51.7 V. For comparison, charge transport properties of single-component single crystals of DPP-PR or C_{60} were also studied. With 40 devices tested, an average μ_h of (0.013 ± 0.003) $cm^2 V^{-1} s^{-1}$ (range: 0.006–0.023, Figure S8 a,c), $I_{on}/I_{off} > 10^4$, and V_T between −66.2 and −81.8 V were achieved for DPP-PR ribbons. While for C_{60} ribbons, we obtained an average μ_e of (0.97 ± 0.42) $cm^2 V^{-1} s^{-1}$ (range: 0.21–1.44, Figure S8b,d), $I_{on}/I_{off} > 10^5$, and V_T between 38.8 and 72.5 V. The mobility values of the donor–acceptor heterojunctions are slightly lower than those based on single-component crystals, possibly due to slight mutual incorporation of the two molecules.

The ambipolar transport property, together with the appropriate energy level alignment (Figure 3b), endows the single-crystalline donor–acceptor heterojunctions with the potential ability to generate photocurrent. In addition, the extended heterojunctions with consistent DPP-PR-top and C_{60}-bottom structure throughout the substrate facilitate solar cell fabrication with an inverted device configuration[14] (Figure 3a). The heterojunctions were grown on freshly prepared ZnO layer on the ITO/glass substrates. Subsequently, a thin layer of MoO_3 was deposited as a hole-transporting layer and a drop of gallium–indium eutectic (EGaIn) was applied as the anode.[15] Photovoltaic measurements were conducted by illuminating the device under a solar simulator with an AM1.5G filter at an intensity of 100 mW cm^{-2}. The typical current density/voltage (*J*–*V*) curve is shown in Figure 3c. A total of 46 devices were tested with the PCE values shown in Figure 3d. An average PCE of (0.255 ± 0.095) % was obtained. For the device with the best performance, a PCE of 0.46 %, a short-circuit current density (J_{SC}) of 2.33 mA cm^{-2}, an open-circuit voltage (V_{OC}) of 0.66 V, and a fill factor (FF) of 29.9 % were achieved. This performance is significantly higher than that of previously reported organic solar cells based on single-crystalline donor–acceptor heterojunctions (PCE of 0.007 % under 1 sun).[7b]

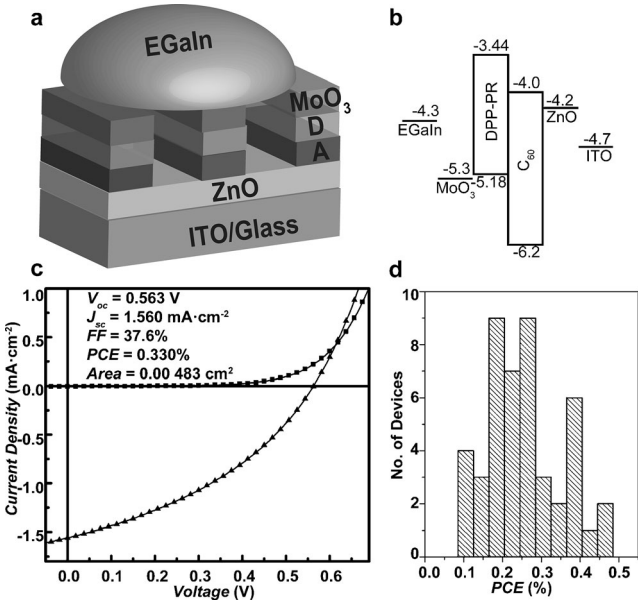

Figure 3. Solar cell performance of the single-crystalline donor–acceptor heterojunctions. a) Schematic configuration of the solar cell device. b) Energy level alignment of the device structures. c) A typical *J*–*V* curve of the single-crystalline donor–acceptor heterojunction solar cell. d) Histogram of PCE values from 46 devices.

Further improvement can be achieved by increasing the light absorption (e.g., using thicker crystals), balancing the hole and electron mobilities, and using electrodes with better electronic contact. In particular, the very unbalanced mobilities of the present donor–acceptor pair will induce the build-up of space-charge and reduce the device performance. High-mobility donors are, therefore, desired.

In summary, a facile solution method to prepare organic single-crystalline donor–acceptor heterojunctions was demonstrated. From a pinned droplet of a mixed solution containing both DPP-PR (donor) and C_{60} (acceptor) molecules, C_{60} and DPP-PR crystallized in a sequential fashion to give extended single-crystalline heterojunctions with consistent DPP-PR-top and C_{60}-bottom structure throughout the substrate. FETs based on the heterojunctions showed ambipolar charge transport behavior with average mobilities of $(0.0026 \pm 0.0015)\ cm^2 V^{-1} s^{-1}$ for holes and $(0.28 \pm 0.12)\ cm^2 V^{-1} s^{-1}$ for electrons. Solar cells based on these donor–acceptor heterojunctions exhibited a high PCE of 0.46%, which is remarkably higher than the previously reported value for a vapor-grown organic single-crystalline donor–acceptor heterojunction. By selecting better donor–acceptor pairs and optimizing of the device structure, the device performance should be further improved. The present work, which outlined a simple solution approach for the preparation of single-crystalline heterojunctions, should accelerate the application of organic single crystals for high-performance photovoltaics. It also provides the possibility of studying emergent physics at organic crystal interfaces.

Experimental Section

DPP-PR was synthesized according to the literature procedure and purified by chromatography on silica gel.[11] Crystals for FETs were grown on a divinyltetramethyldisiloxane–bis(benzocyclobutene) (BCB)-coated[13] highly doped silicon wafer (1 cm^2) with 300 nm thermally oxidized SiO_2, using the DPC method. BCB (Dow Chemicals) thin layers were spin-coated from a mesitylene (Fluka) solution ($V_{BCB}/V_{mesitylene} = 1{:}30$) and then thermally annealed in a N_2 glovebox. A solution (20 μL; DPP-PR, C_{60}, or a mixture of them) was applied dropwise to the substrate. A small piece of the silicon wafer ($0.4 \times 0.4\ cm^2$, pinner) on the substrate was used to pin the solution droplet. The substrate was placed on a Teflon slide inside a Petri- ish (35×10 mm) sealed with parafilm. The crystals were allowed to grow over 2 h on a hotplate (25 ± 1 °C). A mixture of *m*-xylene (Sigma–Aldrich) and carbon tetrachloride (CCl_4, Aladdin; $V_{m\text{-}xylene}/V_{CCl4} = 1{:}1$) was used as solvent. For DPP-PR and C_{60} heterojunctions, a solution with $[DPP\text{-}PR] = 0.4\ mg\,mL^{-1}$ and $[C_{60}] = 0.2\ mg\,mL^{-1}$ was used. In addition, separate single-component ribbon crystals of DPP-PR and C_{60} ($[DPP\text{-}PR] = 0.4\ mg\,mL^{-1}$, $[C_{60}] = 0.2\ mg\,mL^{-1}$) were grown. As a control experiment, crystallization from the mixed solution without using the pinner was carried out. The morphology of the crystals was characterized with OM (Nikon LV100 POL), Raman microscopy (Renishaw InVia Raman Microscope), and AFM (Veeco 3D). Crystal thickness and width were measured by AFM from 10 ribbons. The crystalline structures were examined by SAED (JEOL 1400). Bottom-gate and top-contact FETs were constructed by depositing source and drain electrodes (70 nm Au), with a channel length of 50 μm and a width of 1 mm. The ambipolar characteristics were measured in a N_2 glovebox with a Keithley 4200 semiconductor characterization system. Mobility values were calculated from the saturation regime. The measured capacitance of BCB-coated SiO_2/Si substrates was $10\ nF\,cm^{-2}$ and this value was used for the mobility calculation. For solar cell fabrication, crystals were grown on ZnO-coated substrate. ZnO precursors were spin-coated on cleaned ITO/glass slides (1.5 cm^2) and thermally annealed in air for 15 min.[16] The DPP-PR and C_{60} solution (60 μL, $[DPP\text{-}PR] = 0.4\ mg\,mL^{-1}$, $[C_{60}] = 0.2\ mg\,mL^{-1}$) was applied dropwise and pinned on the freshly prepared ZnO layer allowing the donor–acceptor heterojunctions to grow. The resulting samples were transferred to a vacuum chamber (Angstrom Engineering, below 2×10^{-6} Torr), where 10 nm of MoO_3 was thermally deposited. A drop of EGaIn (contact area: 0.002–0.009 cm^2) was applied on the MoO_3 layer as the anode. The active area of the device was measured by OM. *J*--*V* characteristics were recorded in a N_2 glovebox using a Keithley 2400 source meter and a Newport solar simulator ($100\ mW\,cm^{-2}$, AM 1.5 G) calibrated with a mono-Si photodetector (NREL).

Received: September 8, 2014
Published online: November 25, 2014

Keywords: crystal growth · heterojunctions · organic field-effect transistors · organic photovoltaics · semiconductors

[1] C. W. Tang, *Appl. Phys. Lett.* **1986**, *48*, 183–185.
[2] a) G. Yu, J. Gao, J. C. Hummelen, F. Wudl, A. J. Heeger, *Science* **1995**, *270*, 1789–1791; b) J. J. M. Halls, C. A. Walsh, N. C. Greenham, E. A. Marseglia, R. H. Friend, S. C. Moratti, A. B. Holmes, *Nature* **1995**, *376*, 498–500.
[3] a) P. Peumans, A. Yakimov, S. R. Forrest, *J. Appl. Phys.* **2003**, *93*, 3693–3723; b) R. R. Lunt, N. C. Giebink, A. A. Belak, J. B. Benziger, S. R. Forrest, *J. Appl. Phys.* **2009**, *105*, 053711; c) M. Sim, J. Shin, C. Shim, M. Kim, S. B. Jo, J.-H. Kim, K. Cho, *J. Phys. Chem. C* **2014**, *118*, 760–766; d) D. E. Markov, E. Amsterdam, P. W. M. Blom, A. B. Sieval, J. C. Hummelen, *J. Phys. Chem. A* **2005**, *109*, 5266–5274; e) S. R. Scully, M. D. McGehee, *J. Appl. Phys.* **2006**, *100*, 034907; f) P. E. Shaw, A. Ruseckas, I. D. W. Samuel, *Adv. Mater.* **2008**, *20*, 3516–3520; g) W. A. Luhman, R. J. Holmes, *Adv. Funct. Mater.* **2011**, *21*, 764–771; h) T. K. Mullenbach, K. A. McGarry, W. A. Luhman, C. J. Douglas, R. J. Holmes, *Adv.Mater.* **2013**, *25*, 3689–3693.
[4] a) L. Dou, J. You, Z. Hong, Z. Xu, G. Li, R. A. Street, Y. Yang, *Adv. Mater.* **2013**, *25*, 6642–6671; b) J. You, L. Dou, K. Yoshimura, T. Kato, K. Ohya, T. Moriarty, K. Emery, C.-C. Chen, J. Gao, G. Li, Y. Yang, *Nat. Commun.* **2013**, *4*, 1446; c) V. Gupta, A. K. K. Kyaw, D. H. Wang, S. Chand, G. C. Bazan, A. J. Heeger, *Sci. Rep.* **2013**, *3*, 1965; d) Z. C. He, C. M. Zhong, S. J. Su, M. Xu, H. B. Wu, Y. Cao, *Nat. Photonics* **2012**, *6*, 591–595; e) J. Zhou, Y. Zuo, X. J. Wan, G. Long, Q. Zhang, W. Ni, Y. Liu, Z. Li, G. He, C. Li, B. Kan, M. Li, Y. S. Chen, *J. Am. Chem. Soc.* **2013**, *135*, 8484–8487; f) S.-H. Liao, H.-J. Jhuo, Y.-S. Cheng, S.-A. Chen, *Adv. Mater.* **2013**, *25*, 4766–4771; g) W. Li, A. Furlan, K. H. Hendriks, M. M. Wienk, R. A. J. Janssen, *J. Am. Chem. Soc.* **2013**, *135*, 5529–5532; h) K. Li, Z. J. Li, K. Feng, X. P. Xu, L. Y. Wang, Q. Peng, *J. Am. Chem. Soc.* **2013**, *135*, 13549–13557; i) K. Yao, M. Salvador, C.-C. Chueh, X.-K. Xin, Y.-X. Xu, D. W. deQuilettes, T. Hu, Y. Chen, D. S. Ginger, A. K. Y. Jen, *Adv. Energy Mater.* **2014**, *4*, 1400206; j) W. R. Cao, J. G. Xue, *Energy Environ. Sci.* **2014**, *7*, 2123–2144.
[5] a) R. R. Lunt, J. B. Benziger, S. R. Forrest, *Adv. Mater.* **2010**, *22*, 1233–1236; b) B. Verreet, P. Heremans, A. Stesmans, B. P. Rand, *Adv. Mater.* **2013**, *25*, 5504–5507; c) J. Yang, F. Zhu, B. Yu, H. Wang, D. Yan, *Appl. Phys. Lett.* **2012**, *100*, 103305; d) S. B. Rim, R. F. Fink, J. C. Schoneboom, P. Erk, P. Peumans, *Appl. Phys. Lett.* **2007**, *91*, 173504; e) G. M. Akselrod, P. B. Deotare, N. J. Thompson, J. Lee, W. A. Tisdale, M. A. Baldo, V. M. Menon, V. Bulovic, *Nat. Commun.* **2014**, *5*, 3646.

[6] H. Najafov, B. Lee, Q. Zhou, L. C. Feldman, V. Podzorov, *Nat. Mater.* **2010**, *9*, 938 – 943.
[7] a) B. Yu, L. Huang, H. Wang, D. Yan, *Adv. Mater.* **2010**, *22*, 1017 – 1020; b) Y. J. Zhang, H. L. Dong, Q. X. Tang, S. Ferdous, F. Liu, S. C. B. Mannsfeld, W. P. Hu, A. L. Briseno, *J. Am. Chem. Soc.* **2010**, *132*, 11580 – 11584; c) S. Karak, J. A. Lim, S. Ferdous, V. V. Duzhko, A. L. Briseno, *Adv. Funct. Mater.* **2014**, *24*, 1039 – 1046; d) R. J. Tseng, R. Chan, V. C. Tung, Y. Yang, *Adv. Mater.* **2008**, *20*, 435 – 438; e) J. H. Oh, L. H. Wong, H. Yu, Y. J. Park, J. M. Kim, Z. Bao, *Appl. Phys. Lett.* **2013**, *103*, 053304; f) Q. H. Cui, L. Jiang, C. Zhang, Y. S. Zhao, W. Hu, J. Yao, *Adv. Mater.* **2012**, *24*, 2332 – 2336.
[8] a) V. Podzorov, *MRS Bull.* **2013**, *38*, 15 – 24; b) C. Reese, Z. N. Bao, *Mater. Today* **2007**, *10*, 20 – 27; c) R. J. Li, W. P. Hu, Y. Q. Liu, D. B. Zhu, *Acc. Chem. Res.* **2010**, *43*, 529 – 540.
[9] a) H. Y. Li, B. C. K. Tee, J. J. Cha, Y. Cui, J. W. Chung, S. Y. Lee, Z. N. Bao, *J. Am. Chem. Soc.* **2012**, *134*, 2760 – 2765; b) C. C. Fan, A. P. Zoombelt, H. Jiang, W. F. Fu, J. K. Wu, W. T. Yuan, Y. Wang, H. Y. Li, H. Z. Chen, Z. N. Bao, *Adv. Mater.* **2013**, *25*, 5762 – 5766; c) H. Y. Li, C. C. Fan, M. Vosgueritchian, B. C. K. Tee, H. Z. Chen, *J. Mater. Chem. C* **2014**, *2*, 3617 – 3624.
[10] a) A. B. Tamayo, B. Walker, T.-Q. Nguyen, *J. Phys. Chem. C* **2008**, *112*, 11545 – 11551; b) K. H. Hendriks, G. H. L. Heintges, V. S. Gevaerts, M. M. Wienk, R. A. J. Janssen, *Angew. Chem. Int. Ed.* **2013**, *52*, 8341 – 8344; *Angew. Chem.* **2013**, *125*, 8499 – 8502; c) S. Qu, H. Tian, *Chem. Commun.* **2012**, *48*, 3039 – 3051.
[11] H. Q. Shi, Z. W. Gu, X. Gu, H. B. Pan, J. Y. Pan, X. L. Hu, C. C. Fan, M. M. Shi, H. Z. Chen, *Synth. Met.* **2014**, *188*, 66 – 71.
[12] a) C. Z. Li, H. L. Yip, A. K. Y. Jen, *J. Mater. Chem.* **2012**, *22*, 4161 – 4177; b) Y. Y. Lai, Y. J. Cheng, C. S. Hsu, *Energy Environ. Sci.* **2014**, *7*, 1866 – 1883; c) Y. Li, *Chem. Asian J.* **2013**, *8*, 2316 – 2328.
[13] L. L. Chua, J. Zaumseil, J. F. Chang, E. C. W. Ou, P. K. H. Ho, H. Sirringhaus, R. H. Friend, *Nature* **2005**, *434*, 194 – 199.
[14] S. K. Hau, H. L. Yip, A. K. Y. Jen, *Polym. Rev.* **2010**, *50*, 474 – 510.
[15] D. J. Lipomi, B. C. K. Tee, M. Vosgueritchian, Z. Bao, *Adv. Mater.* **2011**, *23*, 1771 – 1775.
[16] Y. Sun, J. H. Seo, C. J. Takacs, J. Seifter, A. J. Heeger, *Adv. Mater.* **2011**, *23*, 1679 – 1683.

